Multipole method for microstructured optical fibers I: Formulation

T. P. White[1], B. T. Kuhlmey[1,2], R. C. McPhedran[1], D. Maystre[2], G. Renversez[2], C. Martijn de Sterke[1], L.C. Botten[3]

1: School of Physics, University of Sydney, NSW 2006, Australia

2: Institut Fresnel (Unité Mixte de Recherche du CNRS 6133), Faculté des Sciences et Techniques de Saint Jérôme, 13397 Marseille cedex 20, France

3: School of Mathematical Sciences, University of Technology, Sydney, NSW 2008, Australia

October 5, 2001

Abstract

We describe a multipole method for calculating the modes of microstructured optical fibers. The method uses multipole expansions centred on each hole to enforce boundary conditions accurately, and matches expansions with different origins using addition theorems. We also validate the method and give representative results.

1. Introduction

Microstructured optical fibers (MOFs)—fibers with multiple inclusions arranged around the core—have many remarkable properties such as large and adjustable dispersion and nonlinearity[1–4] and single-mode operation over a wide range of wavelengths[5]. They are also of theoretical interest because they incorporate a larger refractive index contrast than conventional fibers, and require a full electromagnetic treatment, rather than the scalar or weak-guidance approximation[6,7]. Since the light confinement is due to many inclusions in a silica matrix rather than a single doped region, the number of degrees of freedom, such as inclusion placement and diameter to spacing ratio, is larger than in conventional fibers.

To develop the potential of MOFs, accurate modeling tools are necessary. A range of methods has been developed, some of which use approximate scalar[5] or vector[8] treatments. A common strategy is to apply in the transverse plane periodic boundary conditions, enforced for example using plane wave expansions[9,10]. However, such supercell treatments effectively replace the necessarily finite MOF structure with an infinite one, and thus cannot address the issue of the loss associated with propagation in a transversely-finite confining structure. Plane-wave methods also do not accommodate general characteristics of the geometry of the inclusions. Whereas they are very general, they are consequently not very efficient.

One method that somewhat accommodates for the shape of the expected modal field expands it in terms of Hermite-Gaussian functions[3,11]. However, these have an intrinsic width, which ideally matches the width of the solution. Hence the method requires some *a priori* knowledge of the solution, which may not be available.

Beam propagation methods use a numerical algorithm to simulate the propagation of a coherent beam along a fiber[12,13], from which the modes and their properties must be extracted *a posteriori*. Both scalar and vector versions are available, and fibers of any geometry can be dealt with. One can calculate modal losses by observing the attenuation upon propagation, but the propagation distance required increases as the loss decreases; this may be important in light of recent experimental work[1] demonstrating very low-loss ($3.2\ \mathrm{dB\,km^{-1}}$) MOFs.

Here we extend multipole formulations for multicore conventional fibers[14,15] to treat MOFs. A key aspect of the method described here is that it makes use of the circularity of the inclusions. It is therefore of high accuracy, converging sufficiently rapidly to be able to treat precisely systems containing quite large numbers of inclusions. The formulation respects accurately the symmetry properties of modes in MOFs having regularly arranged inclusions[16,17], and indeed has been adapted to take into account those symmetry properties to increase computational efficiency. Furthermore, it yields both the real and imaginary parts of the mode propagation constant, the latter giving the geometrical loss associated with the finite extent of the MOFs set of confining inclusions. It can deal with the two types of MOF of current interest: those with a solid core, surrounded with air holes, and those with an air core (a cylindrical hole of somewhat larger radius), again surrounded by air holes, which tend to be more numerous than in the solid core case. Finally, the multipole method has the frequency ω as an input parameter, with the propagation constant β following from the calculation. It is thus well-suited for calculations involving material dispersion. We stress that though we only consider circular inclusions, the multipole method is not necessarily limited to these. Its extention to non-circular inclusions would follow along lines suggested by Felbacq *et al.*[18]

Here we give the basic formulation of the method as well as some results. In a companion paper, to be refered to as II, we discuss the efficient implementation of the method as well as a number of results that are difficult to obtain using other methods and which thus demonstrate the unique features of our method.

2. Multipole Formulation

Our formulation is similar to that of Lo *et al.*[14], who considered the modes of high-index cylindrical inclusions in a low-index background. Therefore, these structures have properly bound modes, irrespective of the geometry. In contrast, here the inclusions have a low index, and these therefore do not support bound modes. Rather, the modes arise from the geometry of the inclusions and, for a finite cladding, they are not bound, but leaky. This difference has important consequences for the method, and we therefore describe it in some detail here. We concentrate on solid core MOFs, with the modifications for air core MOFs discussed in passing.

The geometry we treat is given in Fig. 1, which represents a transverse xy cut of the fibre, which is infinitely extended along the z axis. It shows a silica matrix of (real) refractive index n_e, perforated with a finite number N_c of inclusions indexed by i and of diameter d_i, whose centers are specified by $\mathbf{c}_i$. The refractive index of the inclusions is n_i. In the numerical examples $n_i = 1$, and all inclusions have the same diameter d, except for air-guided MOFs, where the central hole is larger than the others. The air holes are always hexagonally packed and regularly spaced with separation Λ.

Outside this *hole region*, the MOF is enclosed in a jacket (radius $r > R_0$), whose index n_0 may be complex. One possibility is to take a jacket with refractive index of 1, simulating a MOF in air or vacuum. This enables us to investigate modes confined between the microstructured part of the fiber and the air region, as well as effects due to the finite nature of the silica region surrounding fibres. More generally, our method can deal with any type of cladding surrounding the structure.

A. Choice of propagating fields

We characterize in the complex representation the electric and magnetic fields $\boldsymbol{\mathcal{E}}$ and $\boldsymbol{\mathcal{H}}$ in the MOF by specifying the components $\mathcal{E}_z$ and $\mathcal{H}_z$ along the fiber axis, with transverse fields following from from Maxwell's equations[6]. In fact, it is convenient to work with scaled magnetic fields: $\boldsymbol{\mathcal{K}} = Z\boldsymbol{\mathcal{H}}$, where Z denotes the impedance of free space. Each mode is characterized by its propagation constant β, and the transverse dependence of the fields

$$\boldsymbol{\mathcal{E}}(r,\theta,z,t) = \mathbf{E}(r,\theta)e^{i(\beta z-\omega t)} \quad (1)$$

$$\boldsymbol{\mathcal{K}}(r,\theta,z,t) = \mathbf{K}(r,\theta)e^{i(\beta z-\omega t)} \ . \quad (2)$$

with ω denoting the angular frequency, related to the free space wavenumber by $\omega = kc$. Note that β is complex for leaky modes, the imaginary part of β accounting for attenuation along the z axis. Here we will use the modes' *effective index*, which is related to β by $n_{\text{eff}} = \beta/k$.

Each of the fields ($V = E_z$ or $V = K_z$) satisfies the Helmholtz equation

$$(\nabla^2 + (k_\perp^e)^2)V = 0 \quad (3)$$

in the matrix, where $k_\perp^e = \sqrt{k^2 n_e^2 - \beta^2}$, and

$$(\nabla^2 + (k_\perp^i)^2)V = 0 \quad (4)$$

in the holes, where $k_\perp^i = \sqrt{k^2 n_i^2 - \beta^2}$. Care is required when computing complex square roots: For forward propagating modes that attenuate as they propagate in the $+z$ direction, we require $\Re(\beta) > 0, \Im(\beta) > 0$. Assuming for now that $n_0^2 k^2$ is real, and since $k_\perp^J = (k^2 n_0^2 - \beta^2)^{1/2}$, then $\Re(\beta)\Im(\beta) + \Re(k_\perp^J)\Im(k_\perp^J) = 0$, and so $\Re(k_\perp^J)\Im(k_\perp^J) < 0$. Thus $k_\perp^J$ lies in either the second or fourth quadrant of the complex plane. In fact, we must choose the fourth quadrant[6,7] to ensure the outgoing waves have the correct behaviour of taking energy away from the fiber. We treat the case where n_0 has a small imaginary part by continuity.

B. Formulation of the Field Identities

In the vicinity of the l^{th} cylindrical inclusion (see Fig. 1), we represent the fields in the matrix in local coordinates $\mathbf{r}_l = (r_l, \theta_l) = \mathbf{r} - \mathbf{c}_l$ and express the fields in Fourier-Bessel series, a natural basis for harmonic functions in cylindrical coordinates. With $J_m(z)$ and $H_m^{(1)}(z)$ being the usual Bessel function of order m and the Hankel function of the first kind of order m respectively, we have for the electric field

$$E_z = \sum_m \left[A_m^{\mathrm{E}l} J_m(k_\perp^e r_l) + B_m^{\mathrm{E}l} H_m^{(1)}(k_\perp^e r_l)\right] e^{im\theta_l} \quad (5)$$

and similarly for K_z, but with coefficients $A_m^{\mathrm{K}l}$ and $B_m^{\mathrm{K}l}$. In (5) the J_m terms represent the regular incident part $\mathcal{R}^{\mathrm{E}l}$ of the field E_z for cylinder l since it is finite everywhere, while the $H_m^{(1)}$ terms represent the outgoing wave part $\mathcal{O}^{\mathrm{E}l}$ of the field, associated with a source at the center of the cylinder. We thus have $E_z = \mathcal{R}^{\mathrm{E}l} + \mathcal{O}^{\mathrm{E}l}$.

Local expansion (5) is valid only in an annulus extending from the surface of the cylinder to the nearest cylinder or source (region (a) in Fig. 1). The same expression may be used around the jacket boundary which we designate by the superscript 0 (region d in Fig. 1).

Another description of the fields is orginally due to Wijngaard[19]. He reasoned that a field in a region can be written as a superposition of outgoing waves from all source bodies in the region. If the waves originate outside the region, their expansion is in terms of J-type waves, which are source free. Of course this physical argument can be supplemented by rigorous mathematical arguments,[14,19,20] as discussed in Appendix A. For MOFs, the Wijngaard expansion takes the form

$$E_z = \sum_{l=1}^{N_c} \sum_m B_m^{\mathrm{E}l} H_m^{(1)}(k_\perp^e |\mathbf{r}_l|) e^{im \arg(\mathbf{r}-\mathbf{c}_l)} + \sum_m A_m^{\mathrm{E}0} J_m(k_\perp^e r) e^{im\theta} \, . \qquad (6)$$

Each term of the m series is an outgoing wave field with a source at cylinder l, while the final term, indexed by 0, is the regular field originating at the jacket boundary.

Equating (5) and (6), thus enforcing consistency, yields, in the vicinity of cylinder l,

$$\sum_m A_m^{\mathrm{E}l} J_m(k_\perp^e r_l) e^{im\theta_l} = \sum_{\substack{j=1\\ j\neq l}}^{N} \sum_m B_m^{\mathrm{E}j} H_m^{(1)}(k_\perp^e r_j) e^{im\theta_j} + \sum_m A_m^{\mathrm{E}0} J_m(k_\perp^e r) e^{im\theta}, \qquad (7)$$

since the $H_m^{(1)}(k_\perp^e r_l)$ terms are common to both expansions. Evaluating this expression is not straightforward because different terms refer to different origins. We therefore use Graf's addition theorem[21] which lets us transform the origin of the cylindrical waves. A full discussion is given in Appendix B, where we show that it may be viewed as a change of basis transformation. For example the contribution to the local regular field in the vicinity of cylinder l due to cylinder j (line b, Fig. 1) is

$$\sum_n A_n^{\mathrm{E}lj} J_n(k_\perp^e r_l) e^{in \arg(\mathbf{r}_l)} = \sum_m B_m^{\mathrm{E}j} H_m^{(1)}(k_\perp^e r_j) e^{im \arg(\mathbf{r}_j)} \qquad (8)$$

where

$$A_n^{\mathrm{E}lj} = \sum_m \mathcal{H}_{nm}^{lj} B_m^{\mathrm{E}j} \qquad (9)$$

$$\mathcal{H}_{nm}^{lj} = H_{n-m}^{(1)}(k_\perp^e c_{lj}) e^{-i(n-m)\arg(\mathbf{c}_{lj})} \qquad (10)$$

where $\mathbf{c}_{lj} = \mathbf{c}_j - \mathbf{c}_l$, as shown in Appendix B 1. At this point we introduce the notation $\mathbf{A}^{\mathrm{E}lj} = [A_n^{\mathrm{E}lj}]$, that lets us generate vectors of mathematical objects. A similar notation is used for matrices, *i.e.*, $\boldsymbol{\mathcal{H}}^{lj} = [\mathcal{H}_{nm}^{lj}]$. In matrix form, then, we represent the basis change as

$$\mathbf{A}^{\mathrm{E}lj} = \boldsymbol{\mathcal{H}}^{lj} \mathbf{B}^{\mathrm{E}j}. \qquad (11)$$

Similarly, the contribution to the regular incident field at cylinder l due to the jacket (line e, Fig. 1) is

$$\sum_n A_n^{\mathrm{E}l0} J_n(k_\perp^e r_l) e^{in \arg(\mathbf{r}_l)} = \sum_m A_m^{\mathrm{E}0} J_m(k_\perp^e r) e^{im\theta} \qquad (12)$$

where the change of basis (derived in Appendix B 2) is

$$\mathbf{A}^{\mathrm{E}l0} = \boldsymbol{\mathcal{J}}^{l0} \mathbf{A}^{\mathrm{E}0} \qquad (13)$$

with

$$\boldsymbol{\mathcal{J}}^{l0} = \left[\mathcal{J}_{nm}^{l0}\right] = \left[(-1)^{(n-m)} J_{n-m}(k_\perp^e c_l) e^{i(m-n)\arg(\mathbf{c}_l)}\right]. \qquad (14)$$

Accumulating these contributions for all cylinders and the jacket we have, in the annulus (a) around cylinder l (see Fig. 1)

$$\mathbf{A}^{\mathrm{E}l} = \sum_{\substack{j=1\\ j\neq l}}^{N_c} \mathbf{A}^{\mathrm{E}lj} + \mathbf{A}^{\mathrm{E}l0} = \sum_{\substack{j=1\\ j\neq l}}^{N_c} \boldsymbol{\mathcal{H}}^{lj} \mathbf{B}^{\mathrm{E}j} + \boldsymbol{\mathcal{J}}^{l0} \mathbf{A}^{\mathrm{E}0}, \qquad (15)$$

a result that holds for both the E_z and K_z fields.

In a similar way, the outgoing field in the vicinity of the jacket boundary due to cylinder j (line c) is

$$\sum_n B_n^{\mathrm{E}0j} H_n^{(1)}(k_\perp^e r) e^{in\theta} = \sum_m B_m^{\mathrm{E}j} H_m^{(1)}(k_\perp^e r_j) e^{im \arg(\mathbf{r}_j)} \qquad (16)$$

with the change of basis represented by

$$\mathbf{B}^{\mathrm{E}0j} = \boldsymbol{\mathcal{J}}^{0j} \mathbf{B}^{\mathrm{E}j} \qquad (17)$$

where

$$\boldsymbol{\mathcal{J}}^{0j} = \left[\mathcal{J}_{nm}^{0j}\right] = \left[J_{n-m}(k_\perp^e c_l) e^{-i(n-m)\arg(\mathbf{c}_l)}\right]. \qquad (18)$$

as shown in Appendix B 3.

Adding the contributions for all cylinder sources we reexpress the first term on the right-hand side of Wijngaard expansion (6) in a form valid just inside the jacket (region d).

$$\sum_{l=1}^{N_c} \mathcal{O}^{\mathrm{E}l} = \sum_n B_n^{\mathrm{E}0} H_n^{(1)}(k_\perp^e r) e^{in\theta} = \mathcal{O}^{\mathrm{E}0} \qquad (19)$$

where

$$\mathbf{B}^{\mathrm{E}0} = \sum_{l=1}^{N_c} \mathbf{B}^{\mathrm{E}0l} = \sum_{l=1}^{N_c} \boldsymbol{\mathcal{J}}^{0l} \mathbf{B}^{\mathrm{E}l}, \qquad (20)$$

a result that also holds for both E_z and K_z.

C. Boundary Conditions and Field Coupling

While the field identities of the previous section apply individually to each field component, cross coupling between them occurs at boundaries. In what follows, it is most convenient to formulate the boundary conditions in terms of cylindrical reflection coefficients as derived in Appendix C. For circular inclusions, the exterior form, for reflected fields outside each cylinder is

$$\begin{aligned} B_n^{\mathrm{E}l} &= R_n^{\mathrm{EE}l} A_n^{\mathrm{E}l} + R_n^{\mathrm{EK}l} A_n^{\mathrm{K}l} \\ B_n^{\mathrm{K}l} &= R_n^{\mathrm{KE}l} A_n^{\mathrm{E}l} + R_n^{\mathrm{KK}l} A_n^{\mathrm{K}l} \end{aligned} \qquad (21)$$

where the expression for the reflection coefficients are given in Eqs (C11) in Appendix C. The reflection matrices are derived for each inclusion treated in isolation, and are thus known in closed form for circular inclusions, in which case they are diagonal. For non-circular inclusions, they could be replaced by either analytic expressions for other special cases, or numerical estimates from a differential or integral equation treatment[18,22] and they then also have off-diagonal elements.

Equations (21) can be written as

$$\begin{bmatrix} \mathbf{B}^{\mathrm{E}l} \\ \mathbf{B}^{\mathrm{K}l} \end{bmatrix} = \begin{bmatrix} \mathbf{R}^{\mathrm{EE}l} & \mathbf{R}^{\mathrm{EK}l} \\ \mathbf{R}^{\mathrm{KE}l} & \mathbf{R}^{\mathrm{KK}l} \end{bmatrix} \begin{bmatrix} \mathbf{A}^{\mathrm{E}l} \\ \mathbf{A}^{\mathrm{K}l} \end{bmatrix}, \tag{22}$$

or

$$\tilde{\mathbf{B}}^l = \tilde{\mathbf{R}}^l \tilde{\mathbf{A}}^l \tag{23}$$

with $\mathbf{R}^{\mathrm{EE},l} = \mathrm{diag}(R_n^{\mathrm{EE}l})$ and similar definitions for the other reflection matrices. We also need an interior form at the jacket boundary (point d in Fig. 1),

$$\tilde{\mathbf{A}}^0 = \tilde{\mathbf{R}}^0 \tilde{\mathbf{B}}^0 \tag{24}$$

where $\tilde{\mathbf{A}}^0$, $\tilde{\mathbf{B}}^0$ and $\tilde{\mathbf{R}}^0$ are defined as in (22)–(23), and the coefficients of $\tilde{\mathbf{R}}^0$ are given by Eqs (C7). In this form the outgoing field ($\tilde{\mathbf{B}}^0$) generated by all inclusions (line c) is reflected by the jacket to generate the regular field ($\tilde{\mathbf{A}}^0$), which feeds into the incident field for inclusion l (line e in Fig. 1). It is straightforward to adapt $\tilde{\mathbf{R}}^0$ to cases where multiple films surround the hole region.

D. Derivation of the Rayleigh Identity

With the structure of the field coupling derived in the Section 2 C, we now form field identities applying to the vector components $\tilde{\mathbf{A}}^l$ and $\tilde{\mathbf{B}}^l$. From (15) we have

$$\tilde{\mathbf{A}}^l = \sum_{\substack{j=1 \\ j\neq l}}^{N_c} \tilde{\boldsymbol{\mathcal{H}}}^{lj} \tilde{\mathbf{B}}^j + \tilde{\boldsymbol{\mathcal{J}}}^{l0} \tilde{\mathbf{A}}^0 \tag{25}$$

where $\tilde{\boldsymbol{\mathcal{H}}}^{lj} = \mathrm{diag}(\boldsymbol{\mathcal{H}}^{lj}, \boldsymbol{\mathcal{H}}^{lj})$, and $\tilde{\boldsymbol{\mathcal{J}}}^{l0} = \mathrm{diag}(\boldsymbol{\mathcal{J}}^{l0}, \boldsymbol{\mathcal{J}}^{l0})$. Equation (25) is the representation of the regular incident field at cylinder l in terms of outgoing components $\tilde{\mathbf{B}}^j$ from all other cylinders and an incident field contribution $\tilde{\mathbf{A}}^0$ from the jacket.

Combining (25) for all cylinders $l = 1 \ldots N_c$ and introducing $\boldsymbol{\mathcal{A}} = \left[\tilde{\mathbf{A}}^l\right]$ and $\boldsymbol{\mathcal{B}} = \left[\tilde{\mathbf{B}}^l\right]$, we derive

$$\boldsymbol{\mathcal{A}} = \tilde{\boldsymbol{\mathcal{H}}} \boldsymbol{\mathcal{B}} + \tilde{\boldsymbol{\mathcal{J}}}^{\mathrm{B}0} \tilde{\mathbf{A}}^0 \tag{26}$$

where $\tilde{\boldsymbol{\mathcal{H}}} = \left[\tilde{\boldsymbol{\mathcal{H}}}^{lj}\right]$ for $l, j = 1...N_c$ with $\tilde{\boldsymbol{\mathcal{H}}}^{ll} \equiv \mathbf{0}$ and

$$\tilde{\boldsymbol{\mathcal{J}}}^{\mathrm{B}0} = \left[\tilde{\boldsymbol{\mathcal{J}}}^{l0}\right] = \left[(\tilde{\boldsymbol{\mathcal{J}}}^{10})^T,\ (\tilde{\boldsymbol{\mathcal{J}}}^{20})^T,\ \cdots,\ (\tilde{\boldsymbol{\mathcal{J}}}^{N_c 0})^T\right]^T, \tag{27}$$

where the T indicates the transpose. Similarly, the vector outgoing field in the vicinity of the jacket due to all the cylinders is given by

$$\tilde{\mathbf{B}}^0 = \sum_{j=1}^{N_c} \tilde{\boldsymbol{\mathcal{J}}}^{0l} \tilde{\mathbf{B}}^l = \tilde{\boldsymbol{\mathcal{J}}}^{0\mathrm{B}} \tilde{\boldsymbol{\mathcal{B}}} \tag{28}$$

from (20). Here

$$\tilde{\boldsymbol{\mathcal{J}}}^{0\mathrm{B}} = \left[\tilde{\boldsymbol{\mathcal{J}}}^{0l}\right] = \left[\tilde{\boldsymbol{\mathcal{J}}}^{01},\ \tilde{\boldsymbol{\mathcal{J}}}^{02},\ \cdots\ \tilde{\boldsymbol{\mathcal{J}}}^{0N_c}\right] \tag{29}$$

Combining (23), (24), (26) and (28) and eliminating $\tilde{\mathbf{A}}^0$ and $\tilde{\mathbf{B}}^0$ we form a homogeneous system of equations (*Rayleigh identity*) in the source coefficients

$$\left[\mathbf{I} - \boldsymbol{\mathcal{R}}\left(\tilde{\boldsymbol{\mathcal{H}}} + \tilde{\boldsymbol{\mathcal{J}}}^{\mathrm{B}0} \mathbf{R}^0 \tilde{\boldsymbol{\mathcal{J}}}^{0\mathrm{B}}\right)\right] \mathcal{B} \equiv \boldsymbol{\mathcal{M}} \mathcal{B} = \mathbf{0}, \tag{30}$$

where the right-hand side indicates the absence of external sources, and

$$\boldsymbol{\mathcal{R}} = \mathrm{diag}\left[\tilde{\mathbf{R}}^1, \tilde{\mathbf{R}}^2, \cdots, \tilde{\mathbf{R}}^{N_c}\right]. \tag{31}$$

Non-trivial solutions to the homogeneous system (30) correspond to non-zero fields propagating in the z-direction. The solutions represent a non-zero field existing without any exterior source of energy, in other words propagating (possibly leaky) fibre modes.

3. Numerical considerations

A. Mode location

The homogeneous equation (30), the main result of this paper, corresponds to a non-trivial field vector $\boldsymbol{\mathcal{B}}$ only if the determinant of the matrix $\boldsymbol{\mathcal{M}}$ is effectively zero. Once the structure and wavelength are given, the matrix $\boldsymbol{\mathcal{M}}$ depends only on β, or, equivalently, its effective index n_{eff}. The search for modes therefore becomes a matter of finding zeros of the complex function $\det(\boldsymbol{\mathcal{M}})$ of the complex variable n_{eff}. To investigate this numerically, field expansions such as (5) must be truncated, say to have m running from $-M$ to M. In Fig. 2 we show a determinant surface in the neighbourhood of a well defined minimum, corresponding to a mode with a well-characterized propagation constant $n_{\mathrm{eff}} = 1.43858501 + 4.986 \times 10^{-7} i$. This example, and those following, refer to a structure with a single ring of six equally spaced holes with $d = 5$ μm, $\Lambda = 6.75$ μm, $\lambda = 1.45$ μm, and $n_e = 1.45$, $n_0 = n_e + 10^{-8} i$ and $M = 5$.

We know from a group theoretical study of waveguides by McIsaac[16], that the the modes of the fibres we are considering are either nondegenerate or doubly degenerate. Since $\det(\boldsymbol{\mathcal{M}})$ is the product of the eigenvalues of $\mathcal{M}$, we must look for minima in which one or two of the eigenvalues have magnitudes that are substantially smaller than the others. However, a minimum of the determinant may also correspond to more than two eigenvalues being small simultaneously (a *false* minimum). To distinguish these from genuine solutions, we consider the *singular values*[24] of $\mathbf{M}$, which, for our case, correspond to the magnitudes of the eigenvalues. False minima can be distinguished by a singular value decomposition at the putative minimum. Assuming we have a genuine minimum, the accuracy of the singular values may be assessed from the stability of n_{eff} with increasing truncation order. In most cases, the real part of n_{eff} is found to ten decimal places, and the imaginary part to five significant figures, while the ratio of the smallest singular values and the next smallest is about seven orders of magnitude. Another useful diagnostic of false minima is that they often have real n_{eff}, while genuine roots have a non-zero imaginary part. This is further discussed in II.

The null vectors corresponding to small singular values are approximate solutions to the field identity (30). For non-degenerate modes, the null vector is unique to within an arbitrary multiplicative constant. For a two-fold degenerate mode, we let the basis states be prescribed by group theory (see Section 3 B), though any linear combination of these is equally justified.

B. Symmetry properties of modes

McIsaac[16] classified the electromagnetic modes of waveguide structures, according to the symmetry properties of the configuration. The point group most often encountered in MOF studies is C_{6v} since it combines six-fold symmetry with mirror symmetry. This leads immediately to a number of conclusions: any mode belongs to one of eight *classes*, and they are either non-degenerate (classes 1, 2, 7, 8), in which case they exhibit the full symmetry of the structure, or two-fold degenerate (classes 3, 4, 5, 6), in which case they exhibit the full symmetry in an appropriate linear combination. Since the non-degenerate modes have the full symmetry of the structure, their field only needs to be calculated in a *minimum sector* of 30°, the edges of which must coincide with a symmetry axis of the structure, with the field elsewhere following by symmetry. The difference between the modal classes are that different boundary conditions apply to the tangential component of the electric field at the edges of the minimum sector; these are either Neumann ($\partial E_z/\partial\theta = 0$) or Dirichlet ($E_z = 0$) conditions, or combinations of these (see Fig. 3). For the degenerate mode classes the minimum sector is 90° (see Fig. 3).

Table 1 lists the first ten modes for the MOF we are considering, exemplifying all McIsaac's[16] eight mode classes. The losses in dB/km in column 3 are obtained from the imaginary part of n_{eff} by

$$\mathcal{L} = \frac{20}{\ln(10)}\frac{2\pi}{\lambda}\Im(n_{\text{eff}}) \times 10^6, \tag{32}$$

with λ in μm. In Table 1 the losses are large since more than one ring is necessary to achieve losses compatible with practical usage; this is discussed further in II.

We show the fields of the first three modes from Table 1 in Figs. 4–6. Fig. 4 shows a mode with a vertical nodal line for E_z and a horizontal antinodal line. It must therefore belong to class $p = 3$ in Fig. 3, one of a degenerate pair. Its companion ($p = 4$) is shown in Fig. 5. The similarity between $|E_z|$ in Fig. 4 and $|K_z|$ in Fig. 5 is often evident in degenerate MOF modes, but is not exact, since E_z and K_z satisfy different boundary conditions. The non-degenerate mode (Fig. 6) displays the MOF's full six-fold symmetry and has nodes of E_z at angles 0° and 30°; it thus belongs to class $p = 2$ (Fig. 3).

4. Discussion and Conclusions

We have given the basic formulation of our multipole method, and we have shown that it allows one to calculate the modal properties of MOFs. The results presented show the level of detail that can be obtained in calculating field structures and symmetry properties. It is at present limited to designs composed of non-intersecting circular inclusions, but nevertheless it can be employed in studies ranging over a wide parameter space: hole radius, spacing, number of rings, packing geometry, air or solid core, etc. A key feature of the method is that the frequency ω can be used as an input parameter, while the propagation constant β follows from the calculation. This is an important advantage when dealing with dispersive media: Since ω is fixed the appropriate refractive indices are known from the outset. Contrast this with plane wave methods, for example, in which β is fixed and ω follows from the calculation. The appropriate refractive indices are then not known and are usually included using an iterative procedure, considerably adding to the computational requirements.

The magnitude of matrix $\mathcal{M}$ in identity (30) equals $2(2M + 1)N_c$, and is thus moderate if the number of rings is not too large. In addition, as discussed in II, M needs to increase with the size of the holes. We there also detail the method's implementation and validation and also give more numerical results. In light of this we defer further discussions of the method to II.

This work was supported by the Australian Research Council. It also benefited from travel support from the French and Australian Governments.

Appendix A: Derivation of the Wijngaard expansion

To generalize the Wijngaard expansion of the field to MOF, we define a function $U(x, y)$ as

$$U(x,y) = \begin{cases} E_z, & r < R_0, \\ 0, & \text{elsewhere.} \end{cases} \tag{A1}$$

Thus U is continuous inside the hole region, because of the continuity of the tangential field component, while its normal derivative is discontinuous at the boundaries of the inclusions. Both U and its normal derivative are discontinious at the jacket boundary C ($r = R_0$). As a consequence, it can be deduced from (3) and (4) that U satisfies, in the sense of distributions[23],

$$\nabla^2 U + k_\perp^2 U = s \tag{A2}$$

where $k_\perp = k_\perp^i$ in inclusion i, and $k_\perp = k_\perp^e$ elsewhere. Source s is a singular distribution given by

$$s = \sum_{j=1}^{N_c} S_j \delta_{C_j} - T\delta_C - \nabla \cdot (\mathbf{n} Q \delta_C) \tag{A3}$$

with S_j defined at the boundary C_j of the j-th hole as the jump of the normal derivative of U. Further, Q and T are, respectively, the limits of U and its normal derivative at $r = R_0$, where the normal $\mathbf{n}$ is outwardly oriented. The distribution $A\delta_C$ is defined by[23]

$$\langle A\delta_C, \varphi \rangle = \int_C A(M)\varphi(M) dM \tag{A4}$$

M being a point of C, dM the length of an elementary segment of C and φ an infinitely differentiable function with bounded support.

Equation (A2) can be rewritten as

$$\nabla^2 U + (k_\perp^e)^2 U = \left[(k_\perp^e)^2 - (k_\perp)^2\right] U + s \tag{A5}$$

and so in the hole region U follows from the convolution

$$U = G_e \star \left[s + \left((k_\perp^e)^2 - (k_\perp)^2\right) U\right], \tag{A6}$$

where G_e is the Green function of the Helmholtz equation: $G_e = -iH_0^{(1)}(k_\perp^e r)/4$. From (A3) and (A6) U can be reexpressed as

$$U = \sum_{j=1}^{N_c} G_e \star D_j + G_e \star D, \tag{A7}$$

with

$$D_j = S_j \delta_{C_j} + \left[(k_\perp^e)^2 - (k_\perp^j)^2\right] U_j \tag{A8}$$

$$D = -T\delta_C - \nabla \cdot (\mathbf{n} Q \delta_C), \tag{A9}$$

$$U_j = \begin{cases} U \text{ in the } j\text{-th inclusion} \\ 0 \text{ elsewhere.} \end{cases} \tag{A10}$$

Each term $V_j = G_e \star D_j$ of the sum on the right-hand side of (A7) is generated by sources placed inside or at the boundary of the j-th inclusion and satisfies a radiation condition outside this hole. It can be identified at any point outside this inclusion as the field scattered by it. Of course, since it satisfies the homogeneous Helmholtz equation outside the j-th inclusion, in the sense of distributions, it can be represented in the entire matrix region as a Fourier Bessel series

$$V_j = \sum_m B_m^{\mathrm{E}j} H_m^{(1)}(k_\perp^e r_j) e^{im\theta_j}. \tag{A11}$$

The term $G_e \star D$ on the right-hand member of (A7) is generated by sources jacket boundary and it thus has no singularity inside this boundary. It can be identified as the incident field generated by the jacket and illuminating the matrix-inclusion region. It can also be represented in a Fourier Bessel expansion

$$V_{\mathrm{inc}} = \sum_m A_m^{\mathrm{E}0} J_m(k_\perp^e r) e^{im\theta}. \tag{A12}$$

From equations (A7), (A11) and (A12), it can now be shown that in the entire matrix region, the field E_z can be represented by the Wijngaard expansion (6). The same argument can be used for the z component of the magnetic field H_z.

Appendix B: Change of basis

Three changes of basis transformations are required: (i) conversion of outgoing fields sourced on one cylinder to regular fields in the basis of another cylinder; (ii) conversion of the regular field sourced on the jacket boundary to a regular field in the basis of each cylinder; and (iii) conversion of outgoing fields sourced at the cylinders to an outgoing field close to the jacket boundary. These are considered separately below.

1. Cylinder to cylinder conversion

Here we consider an outgoing cylindrical harmonic wave sourced from cylinder j and derive its regular representation in the coordinate system of cylinder l. From Graf's Theorem[21], we derive

$$H_m^{(1)}(k_\perp^e r_j) e^{im \arg(\mathbf{r}_j)} = \sum_{n=-\infty}^{\infty} J_n(k_\perp r_l) e^{in \arg(\mathbf{r}_l)} H_{n-m}^{(1)}(k_\perp^e c_{lj}) e^{-i(n-m)\arg(\mathbf{c}_{lj})}, \tag{B1}$$

so that the total field due to cylinder j is expressed as

$$\sum_{m=-\infty}^{\infty} B_m^j H_m^{(1)}(k_\perp^e r_j) e^{im\arg(\mathbf{r}_j)} = \sum_{n=-\infty}^{\infty} A_n^{lj} J_n(k_\perp^e r_l) e^{in\arg(\mathbf{r}_l)}, \tag{B2}$$

where A_n^{lj}, defined in Eqs (9) and (10), denotes the contribution to the nth multipole coefficient at cylinder l due to cylinder j.

2. Jacket to cylinder conversion

From Graf's Theorem[21] we now have

$$J_m(k_\perp^e r)e^{im\theta} = \sum_{n=-\infty}^{\infty} J_n(k_\perp^e r_l)e^{in\arg(\mathbf{r}_l)}(-1)^{n-m} J_{n-m}(k_\perp^e c_l)e^{-i(n-m)\arg(\mathbf{c}_l)}, \tag{B3}$$

and from this, the change of basis transform is

$$\sum_{m=-\infty}^{\infty} A_m^0 J_m(k_\perp^e r)e^{im\theta} = \sum_{n=-\infty}^{\infty} A^{l0} J_n(k_\perp^e r_l)e^{in\arg(\mathbf{r}_l)}, \tag{B4}$$

where A_n^{l0} denotes the multipole coefficient in the basis of cylinder l due to the regular field radiating from the jacket. Equation (13) is the matrix form (B4).

3. Cylinder to jacket conversion

The relevant transformation from Graf's theorem[21] is now

$$H_m^{(1)}(k_\perp^e r_l)e^{im\arg(\mathbf{r}_l)} = \sum_{n=-\infty}^{\infty} H_n^{(1)}(k_\perp^e r)e^{in\theta} J_{n-m}(k_\perp^e c_l)e^{-i(n-m)\arg(\mathbf{c}_l)}. \tag{B5}$$

The contribution from cylinder l to the outgoing field near the jacket boundary is

$$\sum_{m=-\infty}^{\infty} B_m^l H_m^{(1)}(k_\perp^e r_l)\, e^{im\arg(\mathbf{r}_l)} = \sum_{n=-\infty}^{\infty} B_n^{0l} H_n^{(1)}(k_\perp^e r)\, e^{in\theta}, \tag{B6}$$

which can be written in the matrix notation (17).

Appendix C: Boundary conditions: reflection matrices

We consider a cylinder centered at the origin of refractive index n_- and radius a embedded in a medium of refractive index n_+. To derive the reflection matrices of this cylinder we express the E_z and H_z fields in terms of Fourier-Bessel series in the local cylindrical coordinates (r,θ) inside and outside the cylinder (*c.f.* Eq. (5)),

$$E_z^{\mp}(r,\theta) = \sum_{m=-\infty}^{\infty} \left[A_m^{\mathrm{E}\mp} J_m(k_\perp^{\mp} r) + B_m^{\mathrm{E}\mp} H_m^{(1)}(k_\perp^{\mp} r)\right] e^{im\theta}, \tag{C1}$$

for $r < a$ $(-)$ and $r > a$ $(+)$, with similar expressions for K_z. Here, $k_\perp^{\pm} = (k^{0\,2} n_\pm^2 - \beta^2)^{1/2}$ are the transverse wave numbers inside (outside) the cylinder. We introduce the vectors $\mathbf{A}^{\mathrm{E}\pm} = [A_m^{\mathrm{E}\pm}]$ and $\mathbf{B}^{\mathrm{E}\pm} = [B_m^{\mathrm{E}\pm}]$, as well as their K counterparts, and the condensed notation introduced in Eqs (22) and (23) for $\tilde{\mathbf{A}}^{\pm}$ and $\tilde{\mathbf{B}}^{\pm}$. The interpretation of the J and H terms was given in Section 2. At the cylinder boundary, reflection and transmission occurs and the waves mix with each other, which, because of the linearity of the Maxwell equations, can be expressed as a matrix relation between the various coefficients, as

$$\begin{cases} \tilde{\mathbf{A}}^- = \tilde{\mathbf{T}}^- \tilde{\mathbf{A}}^+ + \tilde{\mathbf{R}}^- \tilde{\mathbf{B}}^-, \\ \tilde{\mathbf{B}}^+ = \tilde{\mathbf{R}}^+ \tilde{\mathbf{A}}^+ + \tilde{\mathbf{T}}^+ \tilde{\mathbf{B}}^-. \end{cases} \tag{C2}$$

Here, $\mathbf{R}^-$ and $\mathbf{R}^+$ are referred to as interior and exterior *reflection matrices* of the cylinder, whereas $\mathbf{T}^+$ and $\mathbf{T}^-$ are transmission matrices, which do not matter in the analysis below. Note that the first of (C2) leads to Eq. (24), whereas the second leads to (23).

The $\mathbf{R}^{\pm}$ matrices can be derived from the continuity of the tangential field components at the cylinder boundary. To do this we need the expressions for the θ components of the fields, which can be expressed as a function of the z components as[6]

$$E_\theta(r,\theta) = \frac{i}{k_\perp^2}\left(\frac{\beta}{r}\frac{\partial E_z}{\partial\theta} - k\frac{\partial K_z}{\partial r}\right), \tag{C3}$$

$$K_\theta(r,\theta) = \frac{i}{k_\perp^2}\left(\frac{\beta}{r}\frac{\partial K_z}{\partial\theta} + kn^2\frac{\partial E_z}{\partial r}\right), \tag{C4}$$

where n is the refractive index. The partial derivatives that appear straightforwardly follow from (C1)

We can now write the continuity conditions for the z components by equating Eqs (C1) on the boundary. Since the resulting equation is valid for all θ, terms with different m decouple and we find for each m

$$A_m^{\mathrm{E}-} J_m^- + B_m^{\mathrm{E}-} H_m^- = A_m^{\mathrm{E}+} J_m^+ + B_m^{\mathrm{E}+} H_m^+, \tag{C5}$$

with the same result for K_z. Here we introduced the condensed notation $J_m^{\pm} = J_m(k_\perp^{\pm} a)$, *etc.*

In the same way we can equate the interior and exterior expressions for E_θ and K_θ. We then obtain two equalities of Fourier series in $e^{im\theta}$, in which, again, terms with different m decouple. These equations, which are not written out here, in combination with (C5) and its K_z counterpart are sufficient to obtain the $\mathbf{R}$ matrices.

We first concentrate on the interior reflection matrix $\tilde{\mathbf{R}}^-$; we obtain its coefficients by setting the exterior incoming field to zero: $\tilde{\mathbf{A}}^+ = \mathbf{0}$. It is now straightforward to solve, for a given m, the linear set of equation given to express $A_m^{\mathrm{E}-}$ and $A_m^{\mathrm{K}-}$ in terms of $B_m^{\mathrm{E}-}$ and $B_m^{\mathrm{K}-}$ by eliminating $B_m^{\mathrm{E}+}$ and $B_m^{\mathrm{K}+}$. We obtain

$$\begin{cases} A_m^{\mathrm{E}-} &= R_m^{\mathrm{EE}^-} B_m^{\mathrm{E}-} + R_m^{\mathrm{EK}^-} B_m^{\mathrm{K}-}, \\ A_m^{\mathrm{K}-} &= R_m^{\mathrm{KE}^-} B_m^{\mathrm{E}-} + R_m^{\mathrm{KK}^-} B_m^{\mathrm{K}-}, \end{cases} \tag{C6}$$

with

$$\begin{aligned} R_m^{\mathrm{EE}-} &= \frac{1}{\delta_m}\Big\{ \left(\alpha^+_{J^-H^+} - \alpha^-_{H^+J^-}\right) \times \\ &\quad \left(n_-^2 \alpha^+_{H^-H^+} - n_+^2 \alpha^-_{H^+H^-}\right) - m^2 J_m^- H_m^- H_m^{+2} \tau^2 \Big\}, \\ R_m^{\mathrm{EK}-} &= \frac{1}{\delta_m}\left\{ \frac{2m\tau}{\pi k a} \frac{k_\perp^+}{k_\perp^-} H_m^{+2} \right\}, \\ R_m^{\mathrm{KE}-} &= -n_-^2 R_m^{\mathrm{EK}-}, \\ R_m^{\mathrm{KK}-} &= \frac{1}{\delta_m}\Big\{ \left(\alpha^+_{H^-H^+} - \alpha^-_{H^+H^-}\right) \times \\ &\quad \left(n_-^2 \alpha^+_{J^-H^+} - n_+^2 \alpha^-_{H^+J^-}\right) + m^2 J_m^- H_m^- H_m^{+2} \tau^2 \Big\}, \end{aligned} \tag{C7}$$

where

$$\alpha^\pm_{J^\pm H^\pm} = \frac{k_\perp^\pm}{k} J_m'^{\pm} H_m^\pm \tag{C8}$$

with other α coefficients defined analogously. Further

$$\begin{aligned} \delta_m &= (\alpha^-_{H^+J^-} - \alpha^+_{J^-H^+})(n_-^2 \alpha^+_{J^-H^+} - n_+^2 \alpha^-_{H^+J^-}) \\ &\quad + (m J_m^- H_m^+ \tau)^2 \end{aligned} \tag{C9}$$

and

$$\tau = \frac{\beta}{a k_\perp^- k_\perp^+}(n_+^2 - n_-^2) \; . \tag{C10}$$

To obtain the exterior reflection matrix $\tilde{\mathbf{R}}^+$ we set $\tilde{\mathbf{B}}^- = \mathbf{0}$, and eliminate the A_m^- coefficients. This yields

$$\begin{aligned} R_m^{\mathrm{EE}-} &= \frac{1}{\delta_m}\Big\{ \left(\alpha^+_{J^-H^+} - \alpha^-_{H^+J^-}\right) \times \\ &\quad \left(n_-^2 \alpha^+_{J^-J^+} - n_+^2 \alpha^-_{J^+J^-}\right) - m^2 J_m^+ H_m^+ H_m^{-2} \tau^2 \Big\}, \\ R_m^{\mathrm{EK}+} &= \frac{1}{\delta_m}\left\{ \frac{2m\tau}{\pi k a} \frac{k_\perp^-}{k_\perp^+} J_m^{-2} \right\}, \\ R_m^{\mathrm{KE}+} &= -n_+^2 R_m^{\mathrm{EK}+}, \\ R_m^{\mathrm{KK}-} &= -\frac{1}{\delta_m}\Big\{ \left(\alpha^+_{J^-J^+} - \alpha^-_{J^+J^-}\right) \times \\ &\quad \left(n_-^2 \alpha^+_{J^-H^+} - n_+^2 \alpha^-_{H^+J^-}\right) - m^2 J_m^+ H_m^+ H_m^{-2} \tau^2 \Big\}. \end{aligned} \tag{C11}$$

1. H. Kubota, K. Suzuki, S. Kawanishi, M. Nakazawa, M. Tanaka, M. Fujita, "Low-loss, 2 km-long photonic crystal fiber with zero GVD in the near IR suitable for picosecond pulse propagation at the 800 nm band", in OSA *Trends in Optics and Photonics* **56**, *Conf. Lasers and Electro-Optics (CLEO2001)*, Technical Digest (Optical Society of America, Washington DC, 2001), CPD3.
2. D. Mogilevtsev, T.A. Birks and P. St. J. Russell, "Group-velocity dispersion in photonic crystal fibres", Opt. Lett. **23**, 1662-1664 (1998).
3. T. M. Monro, D.J. Richardson, N.G.R. Broderick, and P.J. Bennett, "Holey optical fibers: an efficient modal model", J. Lightwave Technol. **17**, 1093-1102 (2000).
4. J.C. Knight, J. Broeng, T.A. Birks, and P. St. Russell, "Photonic band gap guidance in optical fibers," Science **282**,1476-1478 (1998).
5. T.A. Birks, J.C. Knight and P. St. J. Russell, "Endlessly single-mode photonic crystal fibre", Opt. Lett. **22**, 961-963 (1997).
6. A. W. Snyder and J.D. Love, "Optical waveguide theory"(Chapman and Hall, London, 1996).
7. D. Marcuse, *Theory of dielectric optical waveguides* 2$^{\mathrm{nd}}$ ed. (Academic, San Diego, 1991), Ch. 2.
8. M. Midrio, M.P. Singh, and C.G. Someda, "The space filling mode of holey fibres: an analytic vectorial solution" J. Lightwave Technol. **18**, 1031-1048 (2000).
9. A. A. Maradudin and A.R. McGurn, "Out of plane propagation of electromagnetic waves in two-dimensional periodic dielectric medium', J. Mod. Opt. **41**, 275-284 (1994).
10. J. Broeng, T. Sondergaard, S. E. Barkou, P. M. Barbeito, and A. Bjarklev, "Waveguide guidance by the photonic bandgap effect in optical fibre", J. Opt.- Pure Appl Opt. **1**, 477-482 (1999).
11. D. Mogilevtsev, T.A. Birks and P. St. J. Russell, "Localized function method for modeling defect modes in 2-D photonic crystals", J. Lightwave Technol. **17**, 2078-2081 (2000).
12. B.J. Eggleton, P.S. Westbrook, C.A. White, C. Kerbage, R.S. Windeler, and G.L. Burdge, "Cladding-mode-resonances in air-silica microstructure optical fibers," J. Lightwave Technol. **18**, 1084-1100 (2000).
13. J. K. Ranka, R. S. Windeler, and A. J. Stentz, "Optical properties of high-delta air-silica microstructure optical fibres", Opt. Lett. **25**, 796-797 (2000).
14. K.M. Lo, R.C. McPhedran, I.M. Bassett and G. W. Milton,"An electromagnetic theory of dielectric waveguides with multiple embedded cylinders", J. Lightwave Tchnol. **12**, 396-410 (1994).
15. E. Centeno, D. Felbacq, "Rigorous vector diffraction of electromagnetic waves by bidimensional photonic crystals", J. Opt. Soc. Am. A, **17**, 320-327 (2000).
16. P. R. McIsaac, "Symmetry-induced modal characteristics of uniform waveguides-I: Summary of results", IEEE Trans. Microwave Theory Tech. **MTT-23**, 421-429 (1975).
17. M.J. Steel, T. P. White, C.M. de Sterke, R.C. McPhedran, and L.C. Botten, "Symmetry and Degeneracy in

Microstructured Optical Fibres", Opt. Lett. **26**, 488–490 (2001).
18. D. Felbacq, G. Tayeb, and D. Maystre, "Scattering by a random set of parallel cylinders," J. Opt. Soc. Am. A **11**, 2526-2538 (1994).
19. W. Wijngaard, "Guided normal modes of two parallel circular dielectric rods", J. Opt. Soc. Amer. **63**, 944-949 (1973).
20. C-S Chang and H-c Chang, "Theory of the circular harmonics expansion method for multiple-optical-fiber system," J. Lightwave Technol. **12**, 415-417 (1994).
21. M. Abramowitz and I. A. Stegun, *Handbook of mathematical functions* (Dover, New York, 1965).
22. D. Maystre and P. Vincent, "Diffraction d'une onde electromagnetique plane par an object cylindrique non infinitement conducteur," Opt. Comm. **5**, 327-330 (1972).
23. L. Schwartz, *Mathematics for the Physical Sciences* (Addison-Wesley, Reading MA 1966).
24. W.H. Press, B.P.Flannery, S.A. Teukolsky, and W.T. Vetterling, *Numerical Recipes* (Cambridge University Press, Cambridge, 1986), Section 2.9.

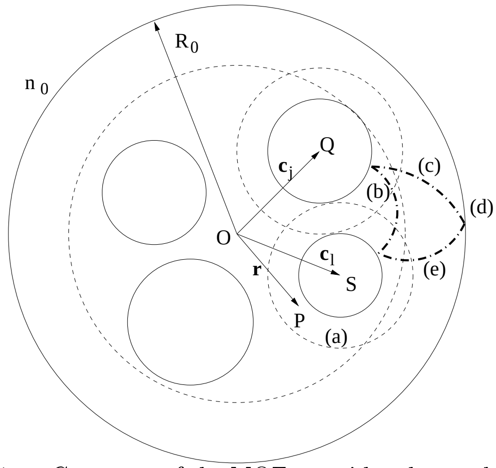

Fig. 1. Geometry of the MOFs considered, together with the contributions to the fields just outside a generic hole i. Regions of convergence of multipole expansions are indicated by dashed lines. Note that QP is $\mathbf{r}_j$ in (8), and SP is $\mathbf{r}_l$ and OP is $\mathbf{r}$. Solid lines indicate physical boundaries, dashed lines indicate regions of convergence.

n_{eff}		Loss	Class	Degeneracy
Real	Imaginary	dB/m	p	
1.445395345	3.15×10^{-8}	1.2	$3,4$	2
1.438585801	4.986×10^{-7}	20	2	1
1.438445842	9.929×10^{-7}	37	$5,6$	2
1.438366726	1.374×10^{-6}	52	1	1
1.430175	2.22×10^{-5}	840	8	1
1.4299694	1.577×10^{-5}	590	$3,4$	2
1.429255296	9.337×10^{-6}	350	7	1

Table 1. Effective index, loss, mode class and degeneracy of the first 10 modes of the MOF given in the text, calculated using $M = 5$.

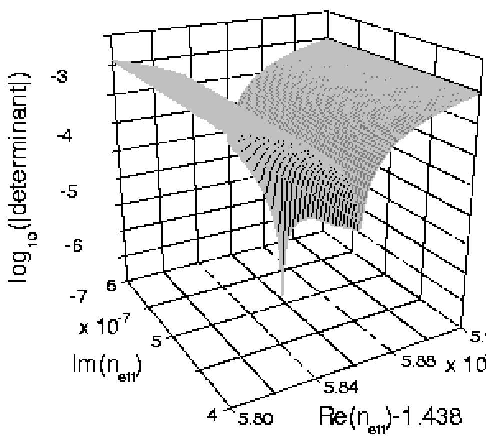

Fig. 2. Logarithm of the magnitude of the determinant of $\boldsymbol{\mathcal{M}}$ versus the real and imaginary parts of the complex refractive index, for the MOF given in the text.

[h]

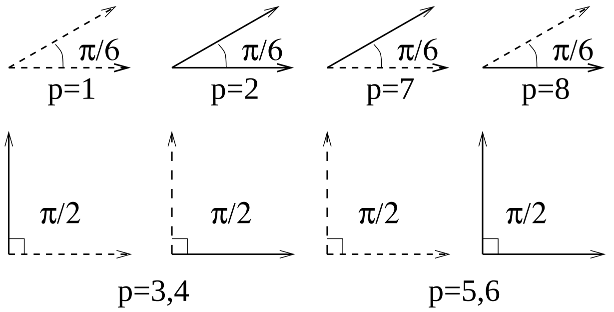

Fig. 3. Minimum sectors for waveguides with C_{6v} symmetry. Mode classes $p = 1, 2, 7$ and 8 are non-degenerate, while $p = 3, 4$ and $p = 5, 6$ are two-fold degenerate. Solid lines indicate Dirichlet boundary conditions for the electric field, dashed lines indicate Neumann boundary conditions.

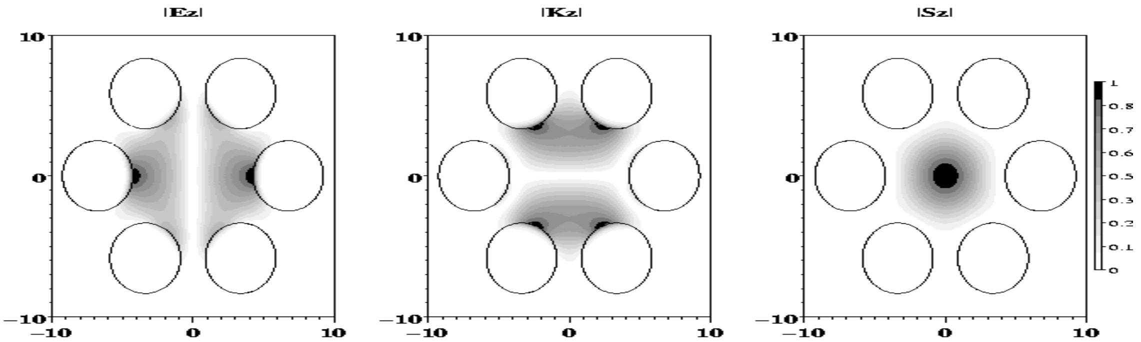

Fig. 4. Fields $|E_z|$, $|K_z|$ and the energy flow S_z for the degenerate fundamental mode class $p = 3$ for a six-hole MOF, with data of Fig. 2. $n_{\mathrm{eff}} = 1.445395345 + 3.15 \times 10^{-8} i$

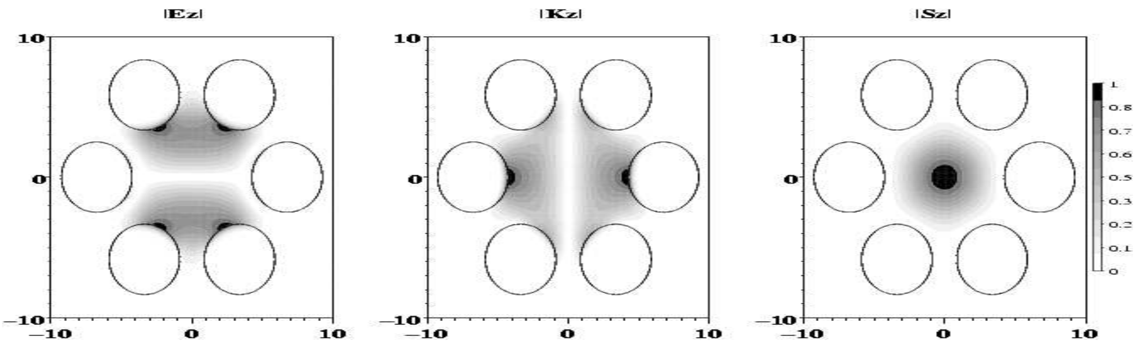

Fig. 5. Similar to Fig 4, but for degenerate fundamental mode class $p = 4$ ($n_{\mathrm{eff}} = 1.445395345 + 3.15 \times 10^{-8} i$).

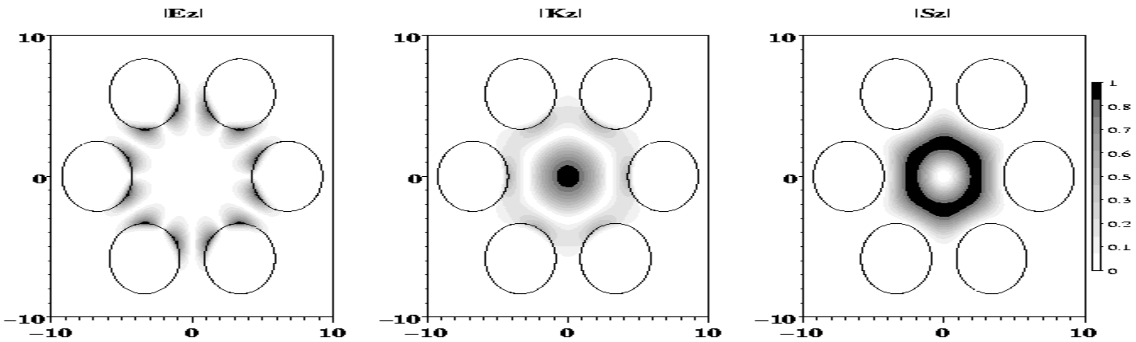

Fig. 6. Similar to Fig 4, but for nondegenerate mode with $p = 2$; $n_{\rm eff} = 1.438585801 + 4.986 \times 10^{-7} i$.